Chinese Journal of Chemical Engineering 53 (2023) 14–24

Contents lists available at ScienceDirect

Chinese Journal of Chemical Engineering

journal homepage: www.elsevier.com/locate/CJChE

Full Length Article

Adsorption dynamics of ethane from air in structured fixed beds with different microfibrous composites

Huan Xiang [1,2], Huiping Zhang [1], Pengfei Liu [1], Ying Yan [1,*]

[1] School of Chemistry and Chemical Engineering, Guangdong Provincial Key Laboratory of Green Chemical Product Technology, South China University of Technology, Guangzhou 510640, China

[2] Energy and Bioproducts Research Institute (EBRI), Aston University, Birmingham B4 7ET, United Kingdom

ARTICLE INFO

Article history:
Received 31 August 2021
Received in revised form 16 November 2021
Accepted 18 November 2021
Available online 27 November 2021

Keywords:
5A zeolite membrane
Microfibrous entrapped activated carbon
Ethane
Structured fixed bed
Adsorption dynamics

ABSTRACT

Adsorption dynamics of ethane in two granular fixed beds and structured fixed beds with microfibrous composites was studied. 5A zeolite membrane 5A/PSSF (paper-like sintered stainless steel fiber) and microfibrous entrapped activated carbon (MEAC) composites were prepared by wet layup papermaking/sintering technique and *in-situ* hydrothermal method. Microfibrous composites were characterized by X-ray diffraction, scanning electron microscopy and N_2 adsorption/desorption. Structured fixed beds were designed by filling granular adsorbents (5A zeolite or activated carbon) and microfibrous composites at the inlet and outlet of the beds, respectively. Effects of flow rate, bed height and structure on the breakthrough curves were investigated. The length of unused bed (LUB) was determined, and Yoon–Nelson model was used to fit the breakthrough curves. The experimental results showed ethane was effectively adsorbed on the granular adsorbents and microfibrous composites. Both composites could decrease the LUB values and enhance bed utilization. All breakthrough curves fitted well to Yoon–Nelson model, with correlation coefficient exceeding 0.89. The adsorption rate of ethane could be improved in the structured fixed beds, which showed an enhanced mass transfer efficiency for ethane adsorption. LUB values of structured fixed beds with 5A/PSSF composites were larger, the bed utilization values were lower, and the adsorption rate constants were higher than those with MEAC composites under the same conditions.

1. Introduction

Air pollution problems have received particular attentions as they can cause huge damage to the environment and human health. Volatile organic compounds (VOCs) are usually regarded as major atmospheric pollutants [1–3]. Among all the VOCs, alkanes are the most prevalent emissions due to their wide use as important feedstocks and transportation fuels [4]. Non-methane VOC hydrocarbons such as ethane are important precursors to tropospheric ozone and aerosols, affecting air quality and climate [5–7]. Ethane is formed and emitted into air as by-products from chemical and petrochemical industries. For example, ethane always appears in the exhaust of natural gas fired combustion turbines and in the epoxidation of ethylene [8]. A continuous increase in ethane emission has been observed during the past decade [5]. To meet with the increasingly stringent targets for permitted levels of atmospheric emissions, the removal of ethane as one of the organic waste gases from air is one of the major challenges.

There are various techniques for organic waste gases abatement, such as condensation, absorption, membrane separation, adsorption and catalytic combustion [9–11]. Among these methods, adsorption is widely used due to its easy operation, high purification efficiency, low energy requirement as well as non-secondary pollution [12,13]. Activated carbon with high specific surface area and adsorption capacity is the most commonly used adsorbent [14]. Zeolites have also been proved to be versatile and promising adsorbents for gas adsorption due to their uniform pore size and high adsorption capacity. Clausse *et al.* [15] studied a temperature swing adsorption process for the removal of different concentrations (0.00035%, 1% and 10%) ethane from air using a carbonaceous adsorbent (Ambersorb 600). All the results showed that ethane could be effectively removed from air to achieve air purification. Puertolas *et al.* [16] investigated the adsorption and desorption process of propane in Na-ZSM-5

* Corresponding author. Fax: +86 2087111975.
E-mail address: yingyan@scut.edu.cn (Y. Yan).

https://doi.org/10.1016/j.cjche.2021.11.009
1004-9541/

zeolite fixed bed by both experimental method and theoretical model. The effects of operation conditions (inlet concentration, temperature and space velocity) on breakthrough curves, desorption cycles and cold start cycles were modeled. The results indicated that Na-ZSM-5 zeolite presented good performance for propane adsorption and the theoretical model was in good agreement with the experimental data.

Besides, microfibrous composites [17–20] (such as microfibrous zeolite membrane and microfibrous entrapped adsorbents) have attracted much attention as novel adsorbents since they have relatively lower bed pressure drop, internal mass transfer resistance and higher adsorption rate compared with granular adsorbents. Nikolajsen *et al.* [21] synthesized an MFI-type (ZSM-5 and silicalite) zeolite film on the surface of the sintered metal fibers (SMF) and developed a novel structured fixed bed with zeolite/SMF composite for purification of low concentration propane as a model VOC compound. Adsorption breakthrough experiments confirmed that zeolite/SMF composite with lower internal diffusion resistance was an efficient adsorbent for VOCs abatement. Chen *et al.* [22,23] compared the adsorption breakthrough behaviors of toluene and isopropanol in granular fixed beds and structured fixed beds with zeolite membrane ZSM-5/PSSF (paper-like sintered stainless steel fiber) composite. It was found that the utilization of bed and mass transfer were significantly enhanced after filling ZSM-5/PSSF composite at the outlet of the structured fixed beds. This indicated that ZSM-5/PSSF composite could be used as a promising adsorbent to effectively minimize the energy cost. Kalluri [24] demonstrated that microfibrous entrapped sorbents could decrease the axial dispersion and increase the radical dispersion and mass transfer rate of adsorbate by hexane breakthrough experiments due to their high voidage and uniform structure.

Although many research works have been focused on the air pollution control and gas purification and great progress has been made, there is no other research paper systematically investigating the adsorption dynamics of ethane from air in both granular fixed beds and structured fixed beds with microfibrous composites, which can provide important guidance for the design of fixed beds for the removal of ethane pollutant from air. Therefore, the aim of this work is to investigate the adsorption dynamics of ethane in granular fixed beds and structured fixed beds with microfibrous composites, and to design fixed beds for ethane adsorption from air with enhanced mass transfer efficiency. For the removal of ethane pollutant from air, 5A zeolite and activated carbon are suitable adsorbents. 5A zeolite have a slightly larger pore size than the kinetic diameter of ethane (0.44 nm), which allows the adsorption of ethane happens while maintaining an excellent ethane adsorption capacity. Besides, the preparation of LTA zeolite membrane on supports (*e.g.*, Al_2O_3) has been successfully developed [25,26]. Activated carbon has high surface area and gas adsorption capacity and has also been used for the synthesis of microfibrous composites. Zeolite membrane 5A/PSSF and microfibrous entrapped activated carbon (MEAC) composites were prepared *via* wet layup papermaking/sintering process and *in-situ* hydrothermal synthesis because the two methods are cheap and easy to operate [27], and the properties of the resulting adsorbent (including the voidage, shape and size of the adsorbent and the membrane thickness of 5A/PSSF and the activated carbon entrapment ratio of MEAC) can be easily adjusted. Adsorption dynamics of ethane from air in the fixed beds was explored by evaluating effects of the flow rate, bed height and bed structure on breakthrough curves. Furthermore, the length of unused bed (LUB) theory and Yoon–Nelson model were used to analyze breakthrough curves for ethane adsorption.

2. Experimental

2.1. Materials

Stainless steel fibers with diameter about 6.5 μm were purchased from Huitong Advanced Material Co., Ltd. Toluene (≥99.5%) was purchased from Guangzhou Chemical Reagent Factory. 3-Aminopropyltrimethoxysilane (APTMS, ≥97%) was purchased from Aladdin Industrial Corporation. Sodium hydroxide (NaOH, ≥96%) and calcium chloride ($CaCl_2$, ≥96%, anhydrous) were purchased from Nanjing Chemical Reagent Co., Ltd. Sodium aluminate ($NaAlO_2$, $Al_2O_3 \geq 41\%$) was purchased from Sinopharm Chemical Reagent Co., Ltd. Colloidal silica LUDOX HS-30 (30% SiO_2 in water) was purchased from Guangzhou Suize Environmental Protection Technology Co., Ltd.

Granular 5A zeolite with an average particle diameter of 3–5 mm was supplied by Tianjin Kermel Reagent Co., Ltd., and commercial columnar activated carbon (AC) with an average particle diameter of 0.9 mm was supplied by Shanxi Xinhua Chemical Plant. The feed gas containing 1% ethane (C_2H_6) in air was supplied by Guangzhou Zhuozheng Gas Co., Ltd.

2.2. Preparation of microfibrous composites

2.2.1. 5A zeolite membrane composite

The schematic diagram for preparation of LTA zeolite membrane on the paper-like sintered stainless steel fiber support was depicted in Fig. 1. There were three steps to synthesize the 5A zeolite membrane composite. Firstly, PSSF support was prepared by the traditional wet layup papermaking and sintering process. Secondly, the PSSF support was treated with APTMS as covalent linker. Finally, 5A zeolite membrane 5A/PSSF composite was fabricated on the surface of PSSF support *via in-situ* hydrothermal synthesis followed by ion exchange. All details of the preparation procedure of PSSF support and 5A zeolite membrane have been reported in the previous work of our group [28].

2.2.2. Microfibrous entrapped activated carbon composite

Microfibrous entrapped activated carbon composite was also prepared by wet layup papermaking and sintering process according to our previous research [29,30]. In this process, granular activated carbon was crushed and sieved to the desired size of 150–180 μm. Stainless steel fibers (6 g), activated carbon particles (13 g) and coniferous wood fibers (1 g, bone dry pulp) were added into water (2 L) and stirred vigorously for 10 min at 50 Hz in a GBJ-A fiber standard dissociation device (Changchun Yueming small testing machine Co., Ltd., China) to form a uniform suspension. The suspension was poured into a ZQJ1-B paper molding machine (Shaanxi University of Science and Technology machinery Factory, China) quickly, and a circular precursor was formed after filtrating. The precursor was then pressed at 400 kPa and dried in air at 110 °C. Finally, the dried precursor was sintered in N_2 at 1050 °C for 30 min to remove the cellulose, and microfibrous entrapped activated carbon composite with three-dimentional network structure was obtained.

The activated carbon entrapment ratio (E, %) of MEAC composite was calculated according to Eq. (1).

$$E = \frac{W_{\mathrm{MEAC}} - W_{\mathrm{F}}}{W_{\mathrm{MEAC}}} \times 100\% \tag{1}$$

where W_{MEAC} (g) and W_{F} (g) are the mass of microfibrous entrapped activated carbon composite and stainless steel fibers, respectively.

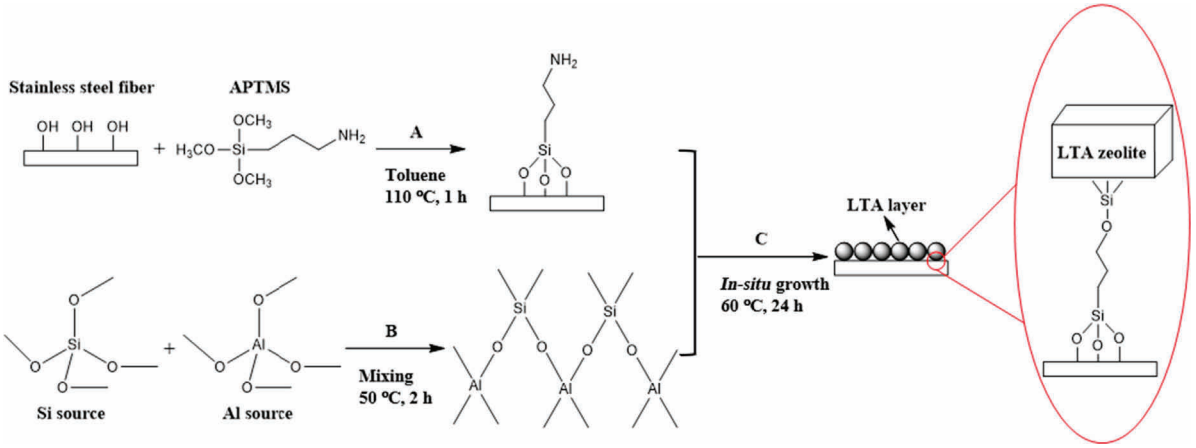

Fig. 1. Schematic diagram for preparation of LTA zeolite membrane on the PSSF support.

2.3. Characterization of microfibrous composites

X-Ray diffraction (XRD) patterns of microfibrous composites were tested on a D8 Advance diffractometer (Bruker, Germany) using Cu K_α radiation source at 40 kV and 40 mA. The data were recorded in the 2θ range of 5°–60° with a step size of 0.02°. The morphologies of the composites were observed by S-3700N scanning electronic microscopy (SEM, Hitachi, Japan). All samples were coated with a gold film to make them to be conductive before analysis. N_2 adsorption–desorption isotherms of the samples were carried out using an ASAP-2020 apparatus (Micromeritics, USA) at −196 °C. All samples were degassed under high vacuum at 200 °C for 2 h before measurements. The obtained N_2 adsorption–desorption isotherms were used to analyze porosity parameters of samples. The specific surface areas (S_{BET}) were calculated by Brunauer–Emmett–Teller (BET) equation. The total volume (V_{total}) and micropore volume (V_{micro}) were determined by *t*-plot method, while the mesopore volume (V_{meso}) was determined by Barrett–Joyner–Halenda (BJH) method. Density functional theory (DFT) method was used to obtain the pore size distribution.

2.4. Adsorption breakthrough experiments

Adsorption breakthrough experiments of ethane in different granular fixed beds and structured fixed beds were performed in a stainless steel tube (2 cm i.d.) at ambient temperature and atmospheric pressure. A schematic diagram of the fixed bed adsorption apparatus was shown in Fig. 2. The breakthrough tests of ethane in individual granular fixed beds were conducted at different feed flow rates and bed heights using a mixture of ethane and air as a test gas. The flow rate varied at 60, 80 and 100 ml·min^{-1}. The bed height varied at 5, 8 and 10 cm in granular 5A zeolite fixed bed, and 3, 4 and 5 cm in granular activated carbon fixed bed. Structured fixed beds with different bed structures were designed. Structured fixed beds were filled with granular adsorbents (5A zeolite or activated carbon with a size of 250–425 μm) with a bed height of 3–5 cm and microfibrous composites (5A/PSSF or MEAC) with a bed height of 2–0 cm at the inlet and outlet, respectively. Adsorption breakthrough experiments of ethane in two different structured fixed beds with 5A/PSSF and MEAC composite were carried out. All adsorbents were dried in oven at 110 °C overnight to remove the physically adsorbed water prior to the experiments. The inlet concentration (C_0) and outlet concentration (C) of ethane were monitored by gas chromatography (g) equipped with a flame ionization detector (FID) and a GS-GasPro capillary column using N_2 as carrier gas. Breakthrough curves are expressed in the form of variations of C/C_0 *versus* time.

3. Theory

3.1. Length of unused bed

It is important to minimize the length of unused bed (LUB) in designing and optimizing an adsorber. LUB represents the length of the mass-transfer zone, which is the part of the fixed bed where the adsorbent is not completely used, and the adsorption is still occurring. The LUB value can be determined by analyzing break-

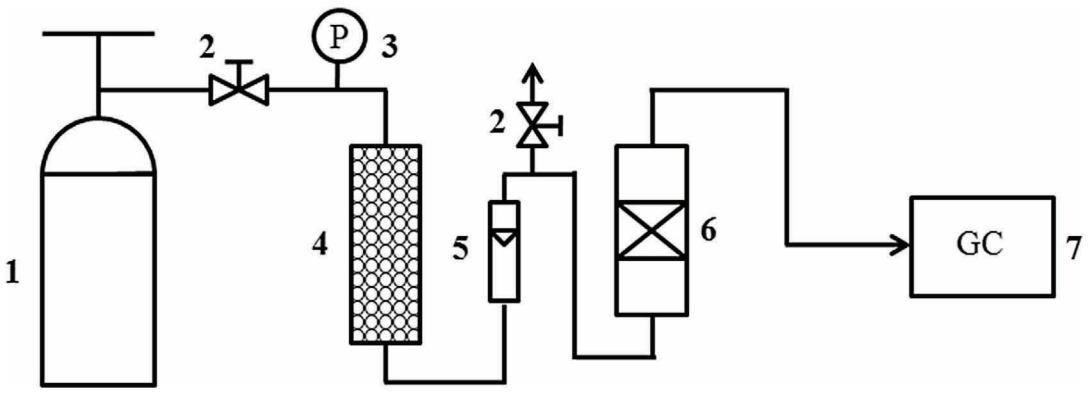

Fig. 2. Schematic diagram of the fixed bed adsorption apparatus: 1. gas cylinder, 2. needle valve, 3. pressure guage, 4. drying column, 5. gas rotameter, 6. fixed bed adsorber, 7. gas chromatograph.

through curves according to the following Eq. (2) developed by Collins [31].

$$\mathrm{LUB} = \left(1 - \frac{t_b}{t^*}\right) L \tag{2}$$

where L (cm) is total bed length, t_b (min) is the breakpoint time when the outlet concentration C (%) equals the breakthrough concentration C_b (0.02% in this work), and t^* (min) is the time at which C/C_0 equals 0.5 for a symmetrical breakthrough curve.

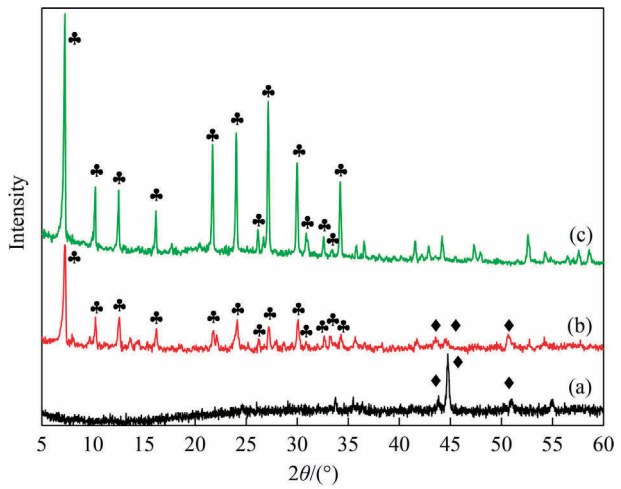

Fig. 3. XRD patterns of samples: (a) PSSF support, (b) 5A/PSSF composite and (c) 5A zeolite. (◆): stainless steel fibers, (♣): 5A zeolite.

The bed utilization (ΔZ, %) can be calculated according to Eq. (3).

$$\Delta Z = \left(1 - \frac{\mathrm{LUB}}{L}\right) \times 100\% \tag{3}$$

3.2. Yoon–Nelson model

Various mathematical models, such as Thomas, Wolborska, Bohart–Adams, bed depth service time (BDST) and Yoon–Nelson models, have been proposed for fitting and analyzing adsorption breakthrough curves [29,32]. Compared with other models, Yoon–Nelson model is less complicated, and requires no details about the properties of adsorbates, the type of adsorbents and the characteristics of adsorption column [33]. Therefore, Yoon–Nelson model is used to describe breakthrough curves for ethane adsorption in this work.

Yoon–Nelson model is based on the assumption that the decrease rate of the adsorption probability for each molecule is proportional to its adsorption and breakthrough probability [34,35]. Yoon–Nelson model used in this study is expressed as Eq. (4).

$$t = \tau + \frac{1}{k'} \ln \frac{C}{C_0 - C} \tag{4}$$

where k' (min^{-1}) is the adsorption rate constant, τ (min) is the time required for 50% ethane breakthrough, t (min) is the sampling time, C (%) is the outlet concentration of ethane, C_0 (%) is the inlet concentration of ethane.

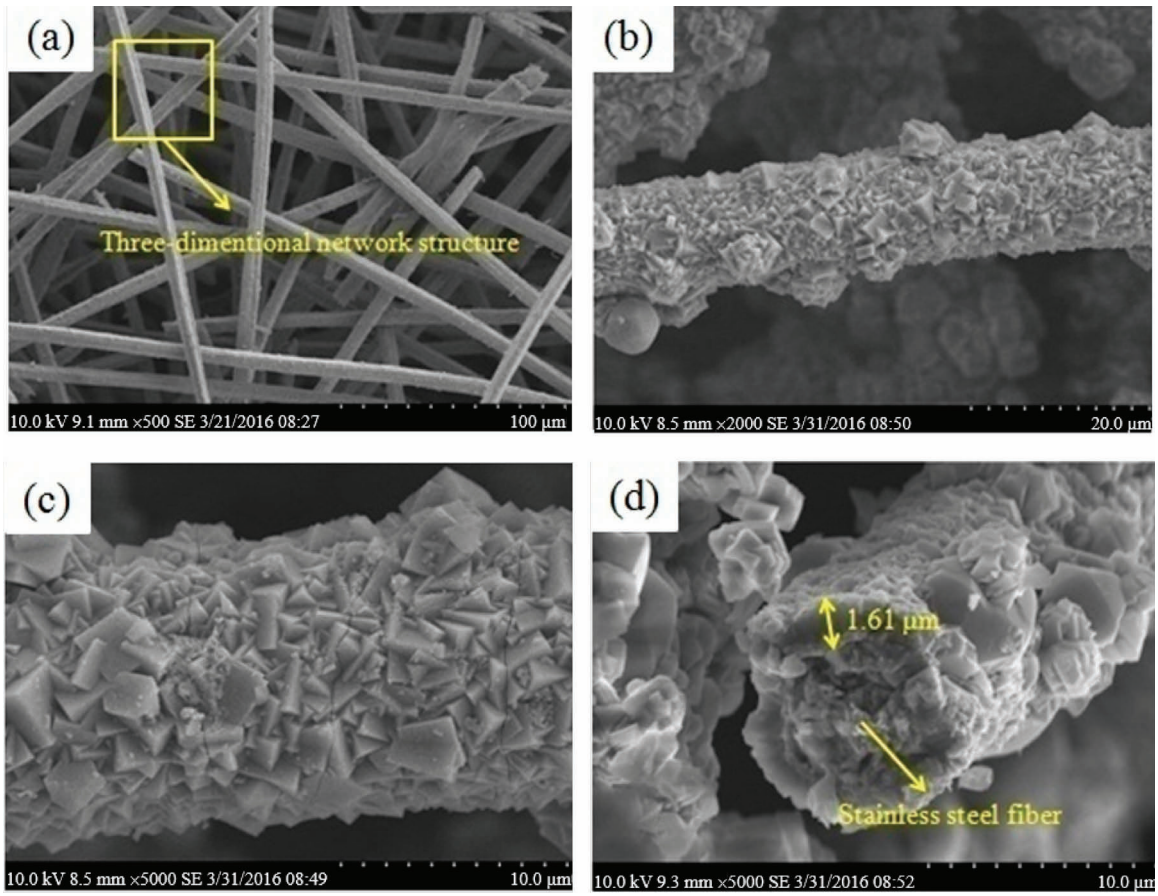

Fig. 4. SEM images of samples: (a) PSSF support at 500×, (b) 5A/PSSF composite at 2000×, (c) 5A/PSSF composite at 5000× and (d) its cross section at 5000×.

4. Results and Discussion

4.1. Characterization of microfibrous composites

4.1.1. XRD

The XRD patterns of PSSF support, 5A/PSSF composite and 5A zeolite are shown in Fig. 3. It can be seen clearly in Fig. 3(a) that there were several diffraction peaks related to the stainless steel fibers at 2θ = 43°–55° [22]. Three of these peaks (marked with ◆) also appeared in the XRD patterns of 5A/PSSF composite in Fig. 3(b). Besides the diffraction peaks attributed to the stainless steel fibers, there were strong diffraction peaks at the range of 2θ = 5°–40° in Fig. 3(b). These peaks (marked with ♣) matched well with those of commercial 5A zeolite powder in Fig. 3(c) and the stand XRD patterns of 5A zeolite [36]. All these results confirmed that 5A zeolite membrane was well crystallized and was successfully fabricated on the surface of the PSSF support.

4.1.2. SEM

The microstructure and morphology of PSSF support and two kinds of microfibrous composites were studied by SEM. Fig. 4 shows the SEM images of PSSF support and zeolite membrane 5A/PSSF. As shown in Fig. 4(a), the junctures of stainless steel fibers were sintered together to form a three-dimensional network structure. Fig. 4(b) and (c) show that the surface of the stainless steel fiber was covered with a continuous and dense 5A zeolite membrane. The thickness of 5A zeolite membrane, detected in the SEM image of the cross section in Fig. 4(d), was about 1.61 μm.

The SEM micrographs of the microfibrous entrapped activated carbon composite before and after sintering are presented in Fig. 5. As shown in Fig. 5(a) and (b), it is obvious that the activated carbon particles in the precursor of MEAC were well entrapped in the network of stainless steel fibers with cellulose as the binder. Fig. 5(c) and (d) show the microstructure of MEAC composite after sintering. Compared with the images of microfibrous composite before sintering, the cellulose observed in Fig. 5(a) and (b) was completely removed after the sintering process, and the junctures of stainless steel fibers were welded together to form a three-dimensional network structure with large voidage. However, activated carbon particles were still entrapped in the sinter-locked network of stainless steel fibers after sintering.

4.1.3. N_2 adsorption–desorption isotherms

The N_2 adsorption–desorption isotherms of 5A zeolite, 5A/PSSF composite, activated carbons and MEAC composite are displayed in Fig. 6. The BET specific surface areas and pore volumes of these samples obtained by analyzing the N_2 adsorption–desorption isotherms are summarized in Table 1. The pore size distributions of zeolite membrane 5A/PSSF and activated carbons before and after sintering are shown in Fig. 7(a) and (b), respectively.

All N_2 adsorption–desorption isotherms in Fig. 6 belongs to type I adsorption isotherm, which indicates that all the samples have a typical microporous feature. At the lower relative pressure, the volume adsorbed increased quickly with increasing relative pressure, which was due to the monolayer adsorption in micropores. As the relative pressure continued increasing, the volume adsorbed increased slowly, which could be ascribed to the multilayer adsorption. An inherent property of Type I adsorption isotherm is that the adsorption is limited to the completion of a single monolayer of adsorbate at the adsorbent surface. Type I adsorption isotherm is observed for the adsorption of gases on microporous solids whose pore sizes are not much larger than the molecular

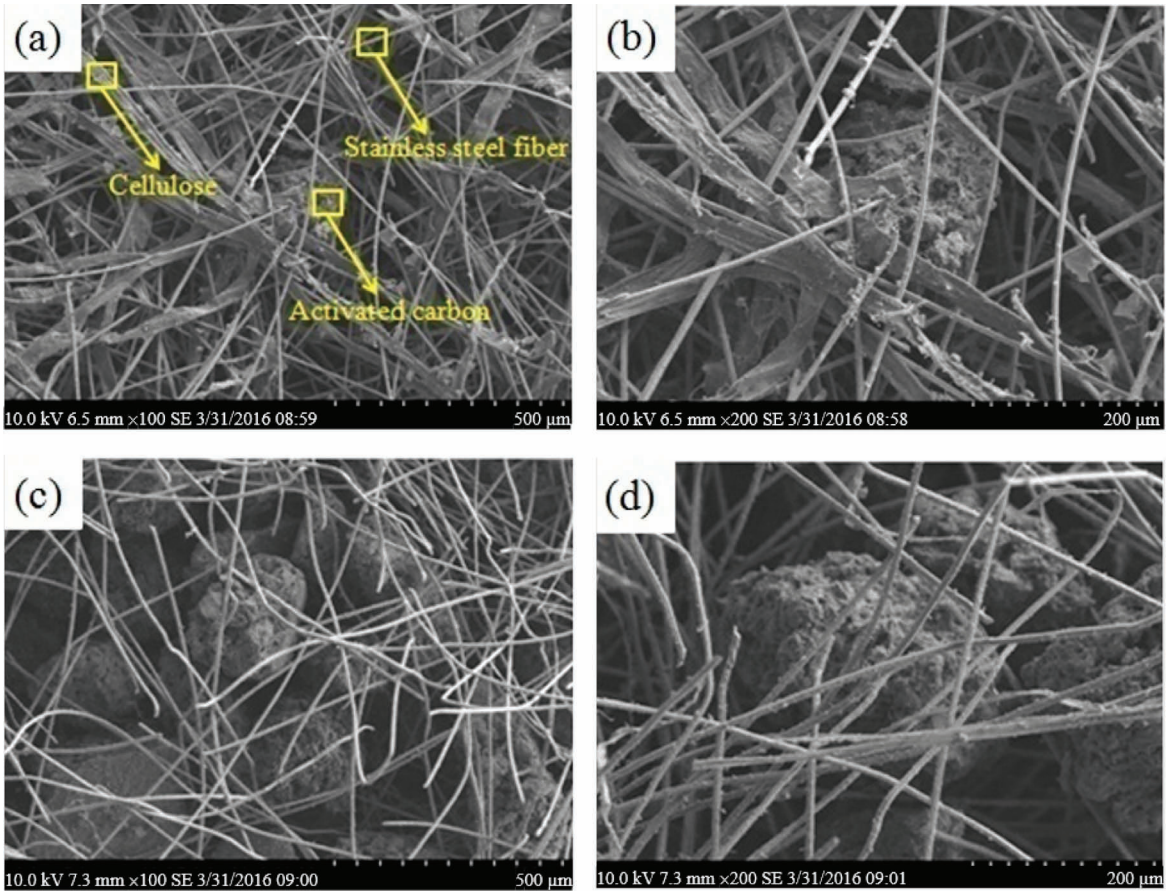

Fig. 5. SEM images of samples: (a) MEAC before sintering at 100×, (b) MEAC before sintering at 200×, (c) MEAC after sintering at 100× and (d) MEAC after sintering at 200×.

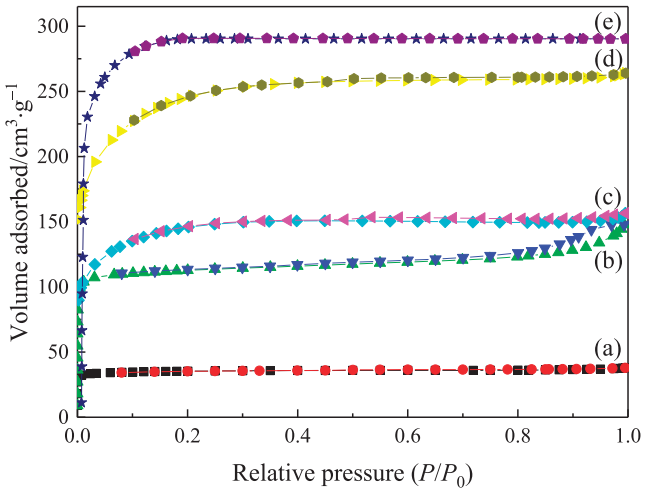

Fig. 6. N_2 adsorption–desorption isotherms of samples at −196 °C: (a) 5A/PSSF composite, (b) 5A zeolite, (c) MEAC composite, (d) activated carbon in MEAC and (e) original activated carbon.

diameter of the adsorbate. Complete filling of these narrow pores corresponds to the completion of a monolayer adsorption. The hysteresis loops observed in Fig. 6(b) at a high relative pressure P/P_0 of 0.8–0.98 may be caused by the existence of the mesopores in 5A zeolite.

As can be seen in Table 1, all the micropore volumes were larger than the corresponding mesopore volumes, which were in good agreement with the obtained N_2 adsorption–desorption isotherms. The BET specific surface area and total pore volume of 5A/PSSF composite were 118 $m^2 \cdot g^{-1}$ and 0.0579 $cm^3 \cdot g^{-1}$, respectively. However, according to our previous research [37], the BET specific surface area and total pore volume of PSSF support are only 12 $m^2 \cdot g^{-1}$ and 5.00×10^{-3} $cm^3 \cdot g^{-1}$. Besides, the pore size distribution of 5A/PSSF composite as shown in Fig. 7(a) was uniform and centered at about 0.5–0.6 nm, which was in good accordance with the theoretical pore size of 5A zeolite powder. Thus, these results confirmed that 5A zeolite membrane had been successfully fabricated on the surface of the PSSF support. As for the MEAC composite, both the specific surface area (457 $m^2 \cdot g^{-1}$) and total pore volume (0.2388 $cm^3 \cdot g^{-1}$) were larger than those of stainless steel fibers, and smaller than those of activated carbons. The activated carbon entrapment ratio of MEAC composite calculated by Eq. (1) was about 64.9%. It can also be known from Table 1 that the specific surface areas of activated carbons before and after sintering were 712 and 786 $m^2 \cdot g^{-1}$, respectively. The specific surface area of activated carbon experienced a slight increase after sintering process. Liu *et al.* [29] had obtained the similar experimental results. The possible reasons are that some carbon particles were further activated, and coniferous wood fibers were carbonized during sintering. In addition, the micropore volume of the original activated carbon was larger than that of activated carbon in MEAC composite, while the mesopore volume became smaller after sintering. These may be due to the pyrolysis of a small part of activated carbon particles and the supplement of activated carbon from carbonized coniferous wood fibers. Moreover, pore size distributions of the original activated carbon and activated carbon in the composite in Fig. 7(b) were similar, and their pore size was mainly centered at 0.5–3.0 nm. However, compared with the height of the peaks of original activated carbon, the height of the peaks around 0.5–1.5 nm of activated carbon in composite was lower, but the height of the peaks at the range of 1.6–3.0 nm became higher. All the findings obtained from Fig. 7(b) were consistent with the results presented in Table 1.

4.2. Adsorption dynamics of ethane in structured fixed beds with different microfibrous composites

4.2.1. Effect of the flow rate

The effects of the feed flow rate on the adsorption breakthrough curves of ethane in granular 5A zeolite fixed beds and activated carbon fixed beds are shown in Fig. 8(a) and (b), respectively. Although these two granular fixed beds were filled with different

Table 1
Pore structure parameters of samples

Sample	S_{BET}/$m^2 \cdot g^{-1}$	V_{micro}/$cm^3 \cdot g^{-1}$	V_{meso}/$cm^3 \cdot g^{-1}$	V_{total}/$cm^3 \cdot g^{-1}$
5A/PSSF	118	0.0485	6.50×10^{-3}	0.0579
5A zeolite	375	0.1528	7.14×10^{-3}	0.2181
MEAC	457	0.1374	5.94×10^{-2}	0.2388
Original activated carbon	712	0.2110	8.61×10^{-2}	0.3793
Activated carbon in MEAC	786	0.2035	10.66×10^{-2}	0.4073

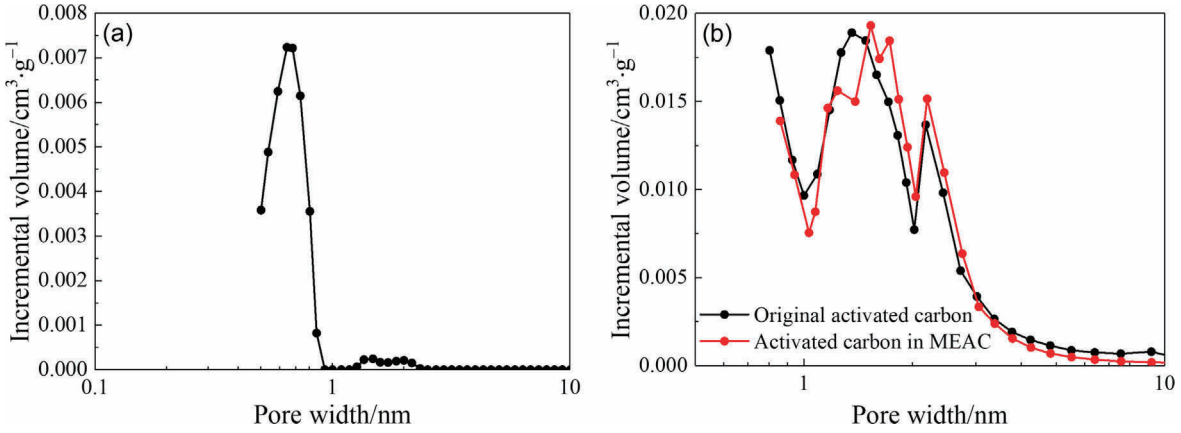

Fig. 7. Pore size distributions of (a) 5A/PSSF composite and (b) original activated carbon and activated carbon in MEAC composite.

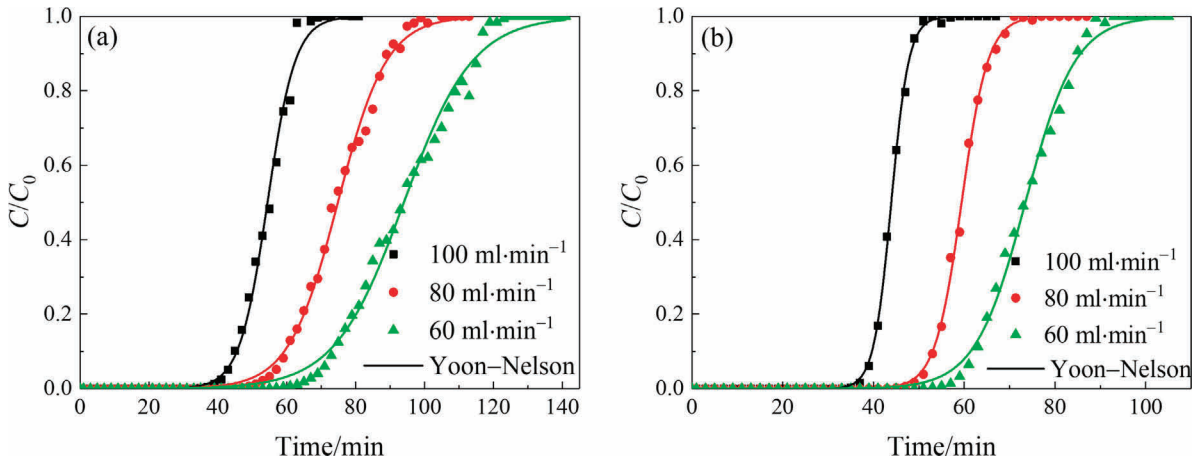

Fig. 8. Breakthrough curves for ethane adsorption in (a) granular 5A zeolite fixed beds at different flow rates (bed height = 10 cm) and (b) granular activated carbon fixed beds at different flow rates (bed height = 5 cm).

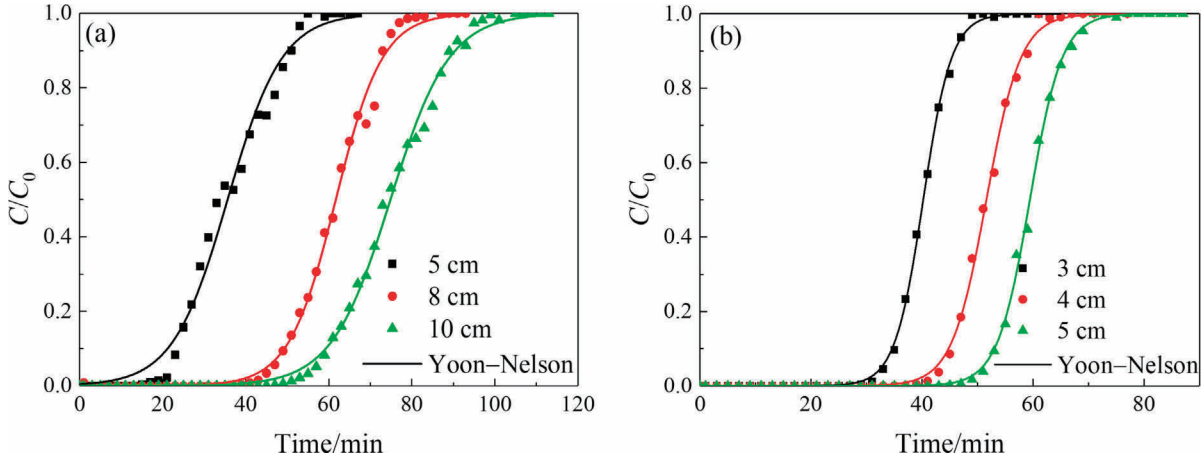

Fig. 9. Breakthrough curves for ethane adsorption in (a) granular 5A zeolite fixed beds at different bed heights (flow rate = 80 ml·min^{-1}) and (b) granular activated carbon fixed beds at different bed heights (flow rate = 80 ml·min^{-1}).

adsorbents, breakthrough curves of ethane in the two beds showed the same trend with the increasing feed flow rate. It can be seen clearly that all breakthrough curves of ethane in Fig. 8(a) and (b) shifted towards the origin and the breakthrough time decreased as the feed flow rate increased. It is because that using relatively higher feed flow rate allows less time for adsorbate (ethane) to interact with adsorbents (5A zeolite and activated carbon), and reduces the time for adsorption to occur, and thus leads to some adsorbate molecules leaving the fixed beds before reaching the adsorption equilibrium. Consequently, this will result in poor utilization of the column capacity. Moreover, at a higher flow rate, the volume of ethane treated per unit time was higher. Therefore, an earlier breakthrough of ethane was observed when higher feed flow rate was tested. In addition, sharper breakthrough curves were obtained at relatively higher flow rate, indicating the adsorption rate of ethane was higher, which was caused by the lower external diffusion resistance in mass transfer.

4.2.2. Effect of the bed height

The effects of the bed height on the adsorption breakthrough curves of ethane in granular 5A zeolite fixed beds and activated carbon fixed beds are shown in Fig. 9(a) and (b), respectively. When the fixed bed height changed, breakthrough curves in 5A zeolite fixed beds as shown in Fig. 9(a) also had the same changing tendency as the breakthrough curves in the activated carbon fixed beds as shown in Fig. 9(b). It can be observed that all breakthrough curves shifted away from the origin with the increasing bed height. At the same time, both the breakthrough time and the time required for complete column saturation increased as bed height increased. It is because that the amount of adsorbents (5A zeolite and activated carbon) filled in the fixed bed adsorber increases with the increasing bed height, and consequently the adsorption capacity of beds is enhanced, which finally results in the increasing breakthrough time of ethane. However, regardless of the variation in the bed height, the slope and steepness of breakthrough curves for ethane adsorption in the two fixed beds almost remained the same. It is due to that axial diffusion coefficient of ethane has nothing to do with the fixed bed height. Hence, it can be concluded that varying in bed height had no impact on the adsorption rate of ethane.

4.2.3. Effect of the bed structure

To investigate the effect of the bed structure on the breakthrough curves, structured fixed beds with different bed structures

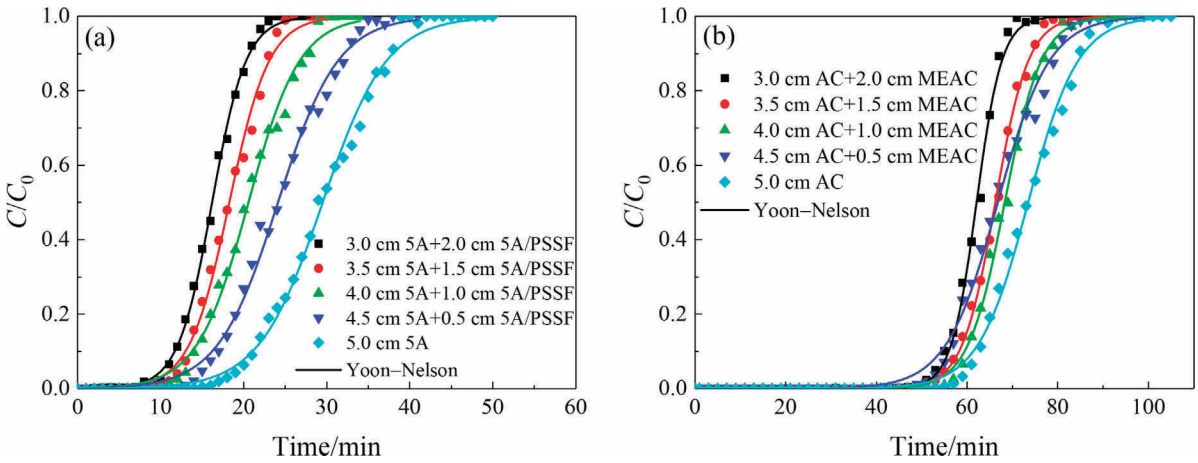

Fig. 10. Breakthrough curves for ethane adsorption in different structured fixed beds with (a) 5A/PSSF composite (total bed height = 5 cm, flow rate = 60 ml·min^{-1}) and (b) MEAC composite (total bed height = 5 cm, flow rate = 60 ml·min^{-1}).

were designed by filling different proportions of granular adsorbents and microfibrous composites in the fixed bed. Structured fixed beds were filled with granular 5A zeolite or activated carbon with a bed height of 3–5 cm at the inlet, and 5A/PSSF or MEAC composite with a bed height of 2–0 cm at the outlet of beds. All breakthrough experiments were measured under the conditions of a total bed height of 5 cm and a flow rate of 60 ml·min^{-1}. The effects of the bed structure on the adsorption breakthrough curves of ethane in the structured fixed beds with 5A/PSSF and MEAC composite are shown in Fig. 10(a) and (b), respectively. Compared with Fig. 10(b), an earlier breakthrough of ethane was observed in structured fixed beds with 5A/PSSF composite (as shown in Fig. 10 (a)) under the same conditions. This result indicated that the adsorption capacity of structured fixed beds with 5A/PSSF composite was smaller than that with MEAC composite at the same filling proportions.

As shown in Fig. 10(a), in the different structured fixed beds with 5A/PSSF composites, all breakthrough curves shifted towards the origin and both the breakthrough time and the time required for complete column saturation decreased with the increasing filling proportion of 5A zeolite membrane composite. When the filling height of 5A/PSSF composite increased from 0 to 2.0 cm, the time for column achieved complete adsorption saturation decreased from 40 to 24 min. Compared with commercial 5A zeolite particles, 5A/PSSF composite has smaller specific surface area and lower adsorption capacity. These are the reasons why the time required for complete column saturation decreased as the filling height of 5A/PSSF composite increased. In granular 5A zeolite fixed bed with a bed height of 5 cm, ethane appeared in the effluent stream at the flow rate of 60 ml·min^{-1} (presented in Fig. 10(a)) earlier than at the flow rate of 80 ml·min^{-1} (presented in Fig. 9(a)). The possible reason is that although all the 5A zeolites were manufactured by the same factory, they might be from different production batches, which led to the difference in their adsorption characteristics. Moreover, breakthrough curves of ethane became sharper with the increasing filling height of 5A/PSSF composite. The result indicated that the adsorption rate of ethane in the structured fixed bed with 5A/PSSF composite was higher compared with that in granular 5A zeolite fixed bed. This is possibly because that 5A/PSSF composite has lower diffusion resistance in mass transfer due to its high voidage. All the experimental results obtained from Fig. 10(a) demonstrated that zeolite membrane 5A/PSSF composite could significantly enhance the contacting efficiency of the adsorbate and adsorbent during the adsorption process.

As shown in Fig. 10(b), in the different structured fixed beds with MEAC composites, all breakthrough curves also shifted towards the origin and the time required for complete column saturation decreased with the increasing filling proportion of microfibrous entrapped activated carbon composite. However, the breakthrough time of ethane did not change regularly due to the nonuniformity of activated carbon entrapment ratio. When the filling height of MEAC composite increased from 0 to 2.0 cm, the time for achieving column saturation decreased from 89 to 71 min. This is also caused by the smaller specific surface area and lower adsorption capacity of MEAC composite compared with activated carbon particles. Besides, filling MEAC composite at the outlet had the same effect on the slope and steepness of breakthrough curves as filling 5A/PSSF composite at the outlet of fixed bed. As the filling proportion of MEAC composite increased, breakthrough curves for ethane adsorption became sharper. This is due to that the particle size of activated carbon entrapped in MEAC composite (150–180 μm) is much smaller than that of granular activated carbon (250–425 μm) filled in the fixed bed, and then the internal diffusion resistance of MEAC composite is lower and the adsorption rate is higher. Therefore, it can be concluded from Fig. 10(b) that microfibrous entrapped activated carbon composite could also enhance the adsorption mass transfer process.

4.3. Determination of LUB

The length of unused bed and bed utilization were calculated by analyzing breakthrough curves of ethane in both individual granular fixed beds and structured fixed beds according to Eqs. (2) and (3). All the values of LUB and ΔZ are listed in Table 2. When the feed flow rate increased from 60 to 100 ml·min^{-1} while other operating parameters were fixed, the changing tendency of LUB and ΔZ of both granular 5A zeolite and activated carbon fixed bed was the same. At a higher flow rate, the LUB value was smaller and bed utilization was higher. However, higher flow rate usually allows insufficient time for adsorption to occur, and then results in lower utilization of fixed bed. The errors of the breakthrough time t_b and t^* are ±1 min. For example, for granular 5A zeolite fixed bed, it gives the values of LUB (2.98 ± 0.18), (2.84 ± 0.23), (2.55 ± 0.32) cm for 60, 80 and 100 ml·min^{-1} flow rate (according to Fig. 9), respectively, and the ΔZ values are (70.2 ± 1.8)%, (71.6 ± 2.3)% and (74.5 ± 3.2)%, respectively. In addition, the selection of the breakthrough concentration C_b affect t_b and thus LUB and ΔZ values. Therefore, the differences between the LUB and ΔZ values at different flow rates are possibly caused by the experimental and

Table 2
LUB and ΔZ for ethane adsorption under different conditions

Fixed bed	F/ml·min^{-1}	t_b/min	t^*/min	LUB/cm	ΔZ/%
10 cm 5A	60	66	94	2.98	70.2
10 cm 5A	80	53	74	2.84	71.6
10 cm 5A	100	41	55	2.55	74.5
8 cm 5A	80	44	62	2.32	71.0
5 cm 5A	80	21	33	1.82	63.6
5 cm 5A	60	17	29	2.07	58.6
4.5 cm 5A + 0.5 cm 5A/PSSF	60	14	24	2.08	58.3
4.0 cm 5A + 1.0 cm 5A/PSSF	60	12	20	2.00	60.0
3.5 cm 5A + 1.5 cm 5A/PSSF	60	11	18	1.94	61.1
3.0 cm 5A + 2.0 cm 5A/PSSF	60	10	16	1.88	62.5
5 cm AC	60	58	73	1.03	79.5
5 cm AC	80	50	60	0.83	83.3
5 cm AC	100	38	44	0.68	86.4
4 cm AC	80	42	52	0.77	80.8
3 cm AC	80	32	40	0.60	80.0
4.5 cm AC + 0.5 cm MEAC	60	52	66	1.06	78.8
4.0 cm AC + 1.0 cm MEAC	60	56	69	0.94	81.2
3.5 cm AC + 1.5 cm MEAC	60	53	67	1.04	79.1
3.0 cm AC + 2.0 cm MEAC	60	51	63	0.95	81.0

calculation errors. When bed height increased, the LUB values of both granular fixed beds nearly remained the same, but the ΔZ values increased. The scale-up of fixed bed in the industrial process is exactly based on this principle.

When the filling height of 5A/PSSF composite in the structured fixed beds increased from 1.0 to 2.0 cm, the LUB value decreased from 2.00 to 1.88 cm, while ΔZ value increased from 60.0% to 62.5%. Only the LUB value (2.08 cm) of the structured fixed bed (4.5 cm 5A + 0.5 cm 5A/PSSF) was slightly larger and ΔZ value (58.3%) was slightly lower than those (2.07 cm and 58.6%) of granular fixed bed (5 cm 5A zeolite). It has been found that the LUB value of the structured fixed bed (3.0 cm 5A + 2.0 cm 5A/PSSF) decreased 9% and ΔZ value increased 7% compared with those of granular fixed bed (5 cm 5A zeolite). In the structured fixed beds with microfibrous entrapped activated carbon composite, when the filling heights of composite were 1.0 and 2.0 cm, the LUB values (0.94 and 0.95 cm) were smaller and ΔZ values (81.2% and 81.0%) were higher than those (1.03 cm and 79.5%) of granular fixed bed (5 cm AC). The LUB values of the two structured fixed beds decreased 9% and 8%, respectively, and both ΔZ values increased 2% compared with those of the corresponding granular fixed bed. Thus, as demonstrated in Table 2, both zeolite membrane 5A/PSSF and MEAC composites can enhance the utilization of fixed bed and reduce the energy costs in adsorption process. Moreover, all breakthrough experiments of ethane in structured fixed beds with two different microfibrous composites were performed under the same conditions. It can be seen obviously that the LUB values of structured fixed beds with 5A/PSSF composites were always larger and ΔZ values were lower than those of structured fixed beds with MEAC composites at the same filling proportions. The result showed that structured fixed beds with MEAC composites had an advantage over structured fixed beds with 5A/PSSF composites for ethane adsorption.

4.4. Yoon–Nelson model

Yoon–Nelson model was applied to analyze breakthrough curves for ethane adsorption in both granular fixed beds and structured fixed beds according to Eq. (4). A linear plot (not shown) of $\ln[C/(C_0-C)]$ *versus* time (t) with slope of k' and intercept of $-k'\tau$ could obtained by the linear regression analysis. The values of k' and τ were determined from the slope and intercept. The values of adsorption rate constants (k'), times required for 50% ethane breakthrough (τ) and corresponding correlation coefficients (R^2) are listed in Table 3.

Table 3
Parameters of Yoon–Nelson model for ethane adsorption under different conditions

Fixed bed	F/ml·min^{-1}	k'/min^{-1}	τ/min	τ_{exp}/min	R^2
10 cm 5A	60	0.0560	95	94	0.9522
10 cm 5A	80	0.0785	75	74	0.9669
10 cm 5A	100	0.1333	54	55	0.9460
8 cm 5A	80	0.0985	62	62	0.9750
5 cm 5A	80	0.0942	36	33	0.8955
5 cm 5A	60	0.1482	29	29	0.9305
4.5 cm 5A + 0.5 cm 5A/PSSF	60	0.1567	25	24	0.9469
4.0 cm 5A + 1.0 cm 5A/PSSF	60	0.1766	21	20	0.9537
3.5 cm 5A + 1.5 cm 5A/PSSF	60	0.2416	18	18	0.9735
3.0 cm 5A + 2.0 cm 5A/PSSF	60	0.2280	16	16	0.9851
5 cm AC	60	0.1093	74	73	0.9533
5 cm AC	80	0.1638	60	60	0.9865
5 cm AC	100	0.2614	44	44	0.9909
4 cm AC	80	0.1688	52	52	0.9761
3 cm AC	80	0.2156	40	40	0.9575
4.5 cm AC + 0.5 cm MEAC	60	0.1026	68	66	0.9648
4.0 cm AC + 1.0 cm MEAC	60	0.1290	69	69	0.9822
3.5 cm AC + 1.5 cm MEAC	60	0.1317	66	67	0.9895
3.0 cm AC + 2.0 cm MEAC	60	0.1704	61	63	0.9779

As can be seen from Table 3, the adsorption rate constant of ethane in both granular fixed beds increased with the increasing feed flow rate. This is because that when the flow rate increased, the external diffusion resistance in adsorption process decreased and thus the adsorption rate constant and mass transfer increased. However, an increasing in the bed height had no significant effect on the value of k'. After filling 5A/PSSF composite at the outlet to form the structured fixed beds, all values of k' were higher than that of granular 5A zeolite fixed bed. As the bed height of 5A/PSSF composite increased from 0 to 1.5 cm, the value of k' gradually increased from 0.1482 to 0.2416 min^{-1}. In other words, the value of k' in the structured fixed bed (3.5 cm 5A + 1.5 cm 5A/PSSF) increased 63% compared with that in the granular fixed bed (5 cm 5A). In the structured fixed beds with MEAC composite, all values of k' except that in the structured fixed bed (4.5 cm AC + 0.5 cm MEAC) were higher than that of granular activated carbon fixed bed. When the bed height of composites increased from 1.0 to 2.0 cm, the value of k' gradually increased from 0.1290 to 0.1704 min^{-1}. After filling 2.0 cm MEAC composite in the structured fixed bed, the value of k' increased 56% compared with that in the corresponding granular fixed bed. Finally, all the above results demonstrated that microfibrous composites had a lower diffusion resistance and could improve the adsorption rate. In addition, the adsorption rate constants of ethane in the structured fixed beds with 5A/PSSF composite were always higher than those in the structured fixed beds with MEAC composite under the same conditions. Since the adsorption rate constant indicated the steepness of breakthrough curves, the values of k' determined by Yoon–Nelson model were in accordance with the breakthrough curves shown in Figs. 8–10.

As for all the 50% breakthrough times determined by Yoon–Nelson model, they were in good agreement with the experimental results (τ_{exp}). Besides, all the correlation coefficients R^2 exceeded 0.89, which also indicated that the model fitted the experimental results well. Furthermore, Yoon–Nelson model was also used to fit the breakthrough curves of ethane. As shown in Figs. 8–10, all the fitting results matched well with experimental data. Therefore, Yoon–Nelson was valid for studying the adsorption dynamics of ethane.

5. Conclusions

The adsorption dynamics of ethane in two fixed beds was investigated by analyzing adsorption breakthrough curves at different flow rates, bed heights and bed structures. All granular adsorbents (5A zeolite and activated carbon) particles and microfibrous composites (5A/PSSF and MEAC) presented good performance for ethane adsorption from air. An increase in flow rate or a decrease in bed height led to an early breakthrough of ethane. Compared with granular fixed beds, the breakthrough curves in structured fixed beds with microfibrous composites were sharper. As the filling proportion of microfibrous composites increased, the breakthrough curves of ethane were sharper.

After filling microfibrous composites at the outlet to form the structured fixed beds, the LUB values could decrease, and the bed utilization and adsorption rate constants could increase. Yoon–Nelson model was found to be suitable for describing all breakthrough curves and determining adsorption parameters (adsorption rate constant and 50% breakthrough time), with all correlation coefficient exceeding 0.89. Besides, the LUB values of structured fixed beds with 5A/PSSF composites were always larger, the bed utilization values were lower, and the adsorption rate constants were higher than those of structured fixed beds with MEAC composites under the same conditions.

Declaration of Competing Interest

The authors declare that they have no known competing financial interests or personal relationships that could have appeared to influence the work reported in this paper.

Acknowledgements

The authors gratefully acknowledge the financial support from the National Natural Science Foundation of China (21776101), and the National Natural Science Foundation of China (22178122) for this work.

References

[1] F.I. Khan, A.K. Ghoshal, Removal of volatile organic compounds from polluted air, *J. Loss Prev. Process. Ind.* 13 (6) (2000) 527–545.
[2] Q. Hu, J.J. Li, Z.P. Hao, L.D. Li, S.Z. Qiao, Dynamic adsorption of volatile organic compounds on organofunctionalized SBA-15 materials, *Chem. Eng. J.* 149 (1–3) (2009) 281–288.
[3] M.S. Li, S.C. Wu, Y.H. Shih, Characterization of volatile organic compound adsorption on multiwall carbon nanotubes under different levels of relative humidity using linear solvation energy relationship, *J. Hazard. Mater.* 315 (2016) 35–41.
[4] B.E. Solsona, T. Garcia, C. Jones, S.H. Taylor, A.F. Carley, G.J. Hutchings, Supported gold catalysts for the total oxidation of alkanes and carbon monoxide, *Appl. Catal. A: Gen.* 312 (2006) 67–76.
[5] D. Helmig, S. Rossabi, J. Hueber, P. Tans, S.A. Montzka, K. Masarie, K. Thoning, C. Plass-Duelmer, A. Claude, L.J. Carpenter, A.C. Lewis, S. Punjabi, S. Reimann, M.K. Vollmer, R. Steinbrecher, J.W. Hannigan, L.K. Emmons, E. Mahieu, B. Franco, D. Smale, A. Pozzer, Reversal of global atmospheric ethane and propane trends largely due to US oil and natural gas production, *Nat. Geosci.* 9 (7) (2016) 490–495.
[6] A.B. Hansen, F. Palmgren, VOC air pollutants in Copenhagen, *Sci. Total Environ.* 189–190 (1996) 451–457.
[7] U. Bedi, S. Chauhan, Modeling the combustion of volatile organic compound (VOC) ethane in monolithic catalytic converter, *Mater. Today: Proc.* 28 (2020) 1727–1731.
[8] S.F. Tahir, C.A. Koh, Catalytic oxidation of ethane over supported metal oxide catalysts, *Chemosphere* 34 (8) (1997) 1787–1793.
[9] R.S. Pillai, I. Khan, E. Titus, C_2-hydrocarbon adsorption in nano-porous faujasite: A DFT study, *Mater. Today: Proc.* 2 (1) (2015) 436–445.
[10] M.C. Campo, A.M. Ribeiro, A.F.P. Ferreira, J.C. Santos, C. Lutz, J.M. Loureiro, A.E. Rodrigues, Carbon dioxide removal for methane upgrade by a VSA process using an improved 13X zeolite, *Fuel Process. Technol.* 143 (2016) 185–194.
[11] B. Ozturk, D. Yilmaz, Absorptive removal of volatile organic compounds from flue gas streams, *Process. Saf. Environ. Prot.* 84 (5) (2006) 391–398.
[12] S. Yun, H. Lee, W.E. Lee, H.S. Park, Multiscale textured, ultralight graphene monoliths for enhanced CO_2 and SO_2 adsorption capacity, *Fuel* 174 (2016) 36–42.
[13] S.P. Deosarkar, V.G. Pangarkar, Adsorptive separation and recovery of organics from PHBA and SA plant effluents, *Sep. Purif. Technol.* 38 (3) (2004) 241–254.
[14] R.T. Yang, Adsorbents: Fundamentals and Applications, John Wiley & Sons, New York, 2003.
[15] M. Clausse, J. Bonjour, F. Meunier, Influence of the presence of CO_2 in the feed of an indirect heating TSA process for VOC removal, *Adsorption* 9 (1) (2003) 77–85.
[16] B. Puértolas, M.V. Navarro, J.M. Lopez, R. Murillo, A.M. Mastral, T. Garcia, Modelling the heat and mass transfers of propane onto a ZSM-5 zeolite, *Sep. Purif. Technol.* 86 (2012) 127–136.
[17] D.K. Harris, D.R. Cahela, B.J. Tatarchuk, Wet layup and sintering of metal-containing microfibrous composites for chemical processing opportunities, *Compos. Part A: Appl. Sci. Manuf.* 32 (8) (2001) 1117–1126.
[18] Y.J. Wang, Y. Tang, X.D. Wang, W. Shan, C. Ke, Z. Gao, J.H. Hu, W.L. Yang, Fabrication of zeolite coatings on stainless steel grids, *J. Mater. Sci. Lett.* 20 (23) (2001) 2091–2094.
[19] E. Reichelt, M.P. Heddrich, M. Jahn, A. Michaelis, Fiber based structured materials for catalytic applications, *Appl. Catal. A: Gen.* 476 (2014) 78–90.
[20] Y. Yang, H.P. Zhang, Y. Yan, Synthesis of CNTs on stainless steel microfibrous composite by CVD: Effect of synthesis condition on carbon nanotube growth and structure, *Compos.B: Eng.* 160 (2019) 369–383.
[21] K. Nikolajsen, L. Kiwi-Minsker, A. Renken, Structured fixed-bed adsorber based on zeolite/sintered metal fibre for low concentration VOC removal, *Chem. Eng. Res. Des.* 84 (7) (2006) 562–568.
[22] H.H. Chen, H.P. Zhang, Y. Yan, Preparation and characterization of a novel gradient porous ZSM-5 zeolite membrane/PSSF composite and its application for toluene adsorption, *Chem. Eng. J.* 209 (2012) 372–378.
[23] H.H. Chen, H.P. Zhang, Y. Yan, Novel gradient porous ZSM-5 zeolite membrane/PSSF composite for enhancing mass transfer of isopropanol adsorption in a structured fixed bed, *Ind. Eng. Chem. Res.* 51 (51) (2012) 16643–16650.

[24] R.R. Kalluri, Microfibrous entrapped catalysts and sorbents: Microstructured heterogeneous contacting systems with enhanced efficiency Ph.D. Thesis, Auburn University, USA, 2008.
[25] A.S. Huang, F.Y. Liang, F. Steinbach, J. Caro, Preparation and separation properties of LTA membranes by using 3-aminopropyltriethoxysilane as covalent linker, *J. Membr. Sci.* 350 (1–2) (2010) 5–9.
[26] A.S. Huang, Q. Liu, N.Y. Wang, X. Tong, B.X. Huang, M. Wang, J. Caro, Covalent synthesis of dense zeolite LTA membranes on various 3-chloropropyltrimethoxysilane functionalized supports, *J. Membr. Sci.* 437 (2013) 57–64.
[27] Y. Yang, K. Yuen Koh, R.Y. Li, H.P. Zhang, Y. Yan, J.P. Chen, An innovative lanthanum carbonate grafted microfibrous composite for phosphate adsorption in wastewater, *J. Hazard. Mater.* 392 (2020) 121952.
[28] D. Zhang, H.P. Zhang, Y. Yan, Synthesis of 5A zeolite coating/PSSF composites and the application for adsorption of methane from air, *RSC Adv.* 5 (68) (2015) 54913–54919.
[29] J. Liu, Y. Yan, H.P. Zhang, Adsorption dynamics of toluene in composite bed with microfibrous entrapped activated carbon, *Chem. Eng. J.* 173 (2) (2011) 456–462.
[30] J. Liu, Y. Yan, H.P. Zhang, Preparation of microfibrous entrapped activated carbon composites and its application for benzene adsorption, *Sep. Sci. Technol.* 49 (13) (2014) 2016–2024.
[31] J. Collins, The LUB/equilibrium section concept for fixed-bed adsorption, *Chem. Eng. Prog. Symp. Ser.* 63 (1967) 31–35.
[32] B. Salamatinia, A.H. Kamaruddin, A.Z. Abdullah, Modeling of the continuous copper and zinc removal by sorption onto sodium hydroxide-modified oil palm frond in a fixed-bed column, *Chem. Eng. J.* 145 (2) (2008) 259–266.
[33] W. Tsai, C. Chang, C. Ho, L. Chen, Adsorption properties and breakthrough model of 1, 1-dichloro-1-fluoroethane on activated carbons, *J. Hazard. Mater.* 69 (1) (1999) 53–66.
[34] Z. Aksu, F. Gönen, Biosorption of phenol by immobilized activated sludge in a continuous packed bed: prediction of breakthrough curves, *Process. Biochem.* 39 (5) (2004) 599–613.
[35] B. Cheknane, M. Baudu, J.P. Basly, O. Bouras, F. Zermane, Modeling of basic green 4 dynamic sorption onto granular organo–inorgano pillared clays (GOICs) in column reactor, *Chem. Eng. J.* 209 (2012) 7–12.
[36] L. Chen, Y.W. Wang, M.Y. He, Q. Chen, Z.H. Zhang, Facile synthesis of 5A zeolite from attapulgite clay for adsorption of *n*-paraffins, *Adsorption* 22 (3) (2016) 309–314.
[37] Y. Yan, S.S. Jiang, H.P. Zhang, X.Y. Zhang, Preparation of novel Fe-ZSM-5 zeolite membrane catalysts for catalytic wet peroxide oxidation of phenol in a membrane reactor, *Chem. Eng. J.* 259 (2015) 243–251.